Actuators Hot Paper

Aggregation-Induced Emissive Carbon Dots Gels for Octopus-Inspired Shape/Color Synergistically Adjustable Actuators

Shuangshuang Wu, Huihui Shi, Wei Lu,* Shuxin Wei, Hui Shang, Hao Liu, Muqing Si, Xiaoxia Le, Guangqiang Yin, Patrick Theato, and Tao Chen*

Abstract: Some living organisms such as the octopus have fantastic abilities to simultaneously swim away and alter body color/morphology for disguise and self-protection, especially when there is a threat perception. However, it is still quite challenging to construct artificial soft actuators with octopus-like synergistic shape/color change and directional locomotion behaviors, but such systems could enhance the functions of soft robotics dramatically. Herein, we proposed to utilize unique hydrophobic carbon dots (CDs) with rotatable surficial groups to construct the aggregation-induced emission (AIE) active glycol CDs polymer gel, which could be further employed to be interfacially bonded to an elastomer to produce anisotropic bilayer soft actuator. When putting the actuator on a water surface, glycol spontaneously diffused out from the gel layer to allow water intake, resulting in a color change from a blue dispersion fluorescence to red AIE and a shape deformation, as well as a large surface tension gradient that can promote its autonomous locomotion. Based on these findings, artificial soft swimming robots with octopus-like synergistic shape/color change and directional swimming motion were demonstrated. This study provides an elegant strategy to develop advanced multi-functional bio-inspired intelligent soft robotics.

Introduction

In nature, many living creatures have evolved to take full advantage of synergistic shape deformation, color change and directional locomotion for the purpose of communicating, disguising or even intimidating in their environments.[1] One well-known example is the octopus. When there is a threat perception, octopi will make a funnel in the lower part of their head to spray water that pushes their body to swim away, while simultaneously altering their shape and skin colors to blend into the surrounding environment[1f] (Scheme 1a). These marvelous multi-function synergistic behaviors 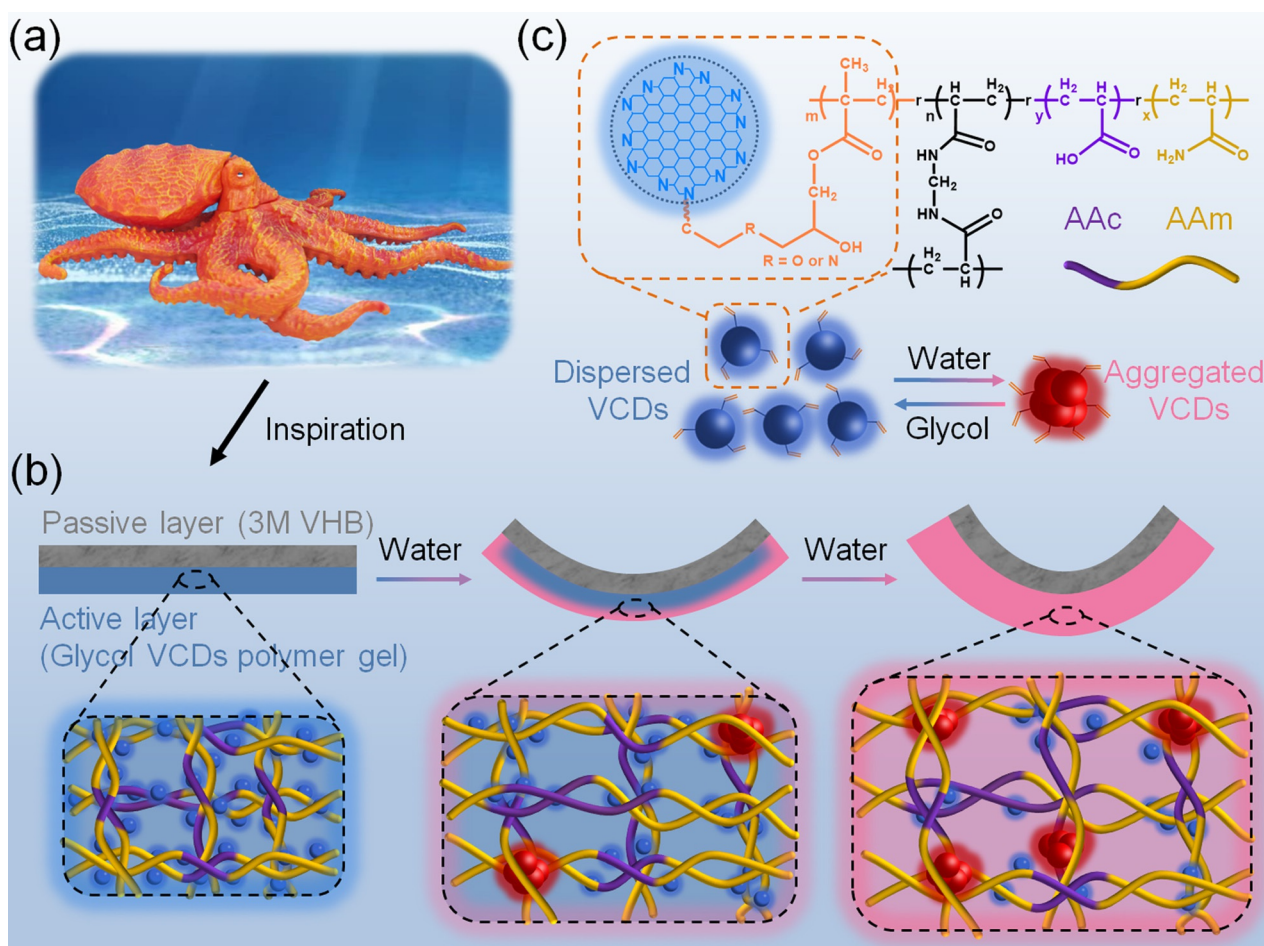of natural systems have long been envisaged to be replicated by artificial soft materials, especially soft wet polymer gels with biotissue-like mechanical properties.[2,3] Such studies will not only be beneficial to the understanding of natural multi-function synergistic behaviors, but also potentially make bio-inspired multifunctional robots/machines accessible.[4] For example, Tang et al.[3k] presented a pH-controlled aggregation-induced emissive bilayer hydrogel actuator that has the desirable ability to show flower-like simultaneous color change and shape deformation. Very recently, Mei and colleagues[4i] utilized a dynamic wetting process of stimuli-responsive active polymer hydrogels via Marangoni effect to realize an remarkable water strider-like deformable locomotion on the surface of water. These developments are very impressive, as they enabled the successful replication of bifunctional biological behaviors (color/shape change or deformation/locomotion) in artificial soft gel systems.[5] However, it is still quite challenging to realize the tri- or multi-functional synergy of higher living organisms, such as the more complex synergistic shape deformation, color change and directional locomotion of octopi, because more delicate material design, but not only simple component combination, is required for adding one more function.

As such, the emerging carbon dots (CDs) polymer gels provide an ideal material platform for developing such trifunctional bioinspired intelligent systems, owing to their good biocompatibility, eco-friendly and facile structure, as well as composition modulation.[6,7] So far, CDs polymer gels have demonstrated many potential applications in sensing, encryption, and optoelectronic devices.[8,9] Unfortunately, this promising kind of new materials with unique luminescent characteristics have not been explored for applications in soft robotics, but such studies could enhance the functions of certain artificial machines. This might be due to the following reasons: (1) Most reported CDs polymer gels suffered from the π-π stacking aggregation of CDs' large conjugated systems, which is prone to consume the transition energy to

[*] S. Wu, H. Shi, Prof. W. Lu, S. Wei, H. Shang, H. Liu, M. Si, Dr. X. Le, Dr. G. Yin, Prof. T. Chen
Key Laboratory of Marine Materials and Related Technologies, Zhejiang Key Laboratory of Marine Materials and Protective Technologies, Ningbo Institute of Materials Technology and Engineering, Chinese Academy of Sciences
Ningbo 315201 (P. R. China)
and
School of Chemical Sciences, University of Chinese Academy of Sciences, 19A Yuquan Road, Beijing 100049 (P. R. China)
E-mail: luwei@nimte.ac.cn
tao.chen@nimte.ac.cn

Prof. P. Theato
Soft Matter Synthesis Laboratory, Institute for Biological Interfaces III, Karlsruhe Institute of Technology (KIT)
Hermann-von-Helmholtz-Platz 1, 76344 Eggenstein-Leopoldshafen (Germany)
and
Institute for Chemical Technology and Polymer Chemistry, Karlsruhe Institute of Technology (KIT)
Engesser Str. 18, 76131 Karlsruhe (Germany)

Supporting information and the ORCID identification number(s) for the author(s) of this article can be found under:
https://doi.org/10.1002/anie.202107281.

21890 Wiley Online Library

© 2021 Wiley-VCH GmbH

Angew. Chem. Int. Ed. **2021**, 60, 21890–21898

Scheme 1. a) Scheme of the octopus with tri-function synergistic behaviors, that is, simultaneous shape deformation, color change and directional locomotion. When there is a threat perception, octopus will make the funnel in the lower part of its head to spray water that pushes it's body to swim away, while simultaneously alter its shape and skin color to blend into the surrounding environment. b) Schematic illustration of the synergistic shape and fluorescence color changes of the bilayer glycol VCDs polymer gel/3 M VHB actuator in water and the involved mechanism. c) Chemical structure of the VCDs polymer gel and schematic representation of the reversible two-switch-mode fluorescence (blue dispersed fluorescence and red AIE).

result in aggregation-caused-quenching (ACQ) of the CDs' fluorescence. Therefore, the concentration of CDs doped in the polymer network is usually limited in order to block the CDs from direct contact and eliminate the adverse effect of ACQ. (2) These CDs polymer gels showed only an "on-off" fluorescence switching behavior, which is far inferior to that of octopi, who are capable of displaying variable skin colors. (3) The present CDs gels usually have isotropic structures. Therefore, they normally exhibited stimuli-responsive homogeneous shrinking/swelling behaviors, which restricts their potential to accomplish complex 3D shape deformation/ movements.

In this study, we propose to take advantage of CDs with rotatable symmetric surfaces to develop aggregation-induced emissive CDs polymer gels with reversible two-switch-mode fluorescence, followed by the fabrication of anisotropic swimming robot showing octopus-like synergistic shape/color change and autonomous locomotion on the water surface. Inspired by the design of classic organic AIE luminogens,[10] the vinyl-functionalized CDs (VCDs) were specially designed

to be crowned with rotatable hydrophobic surficial groups on the basis of a reported synthesis method.[10c] The blue fluorescent glycol VCDs polymer gels were then prepared by radical copolymerization of acrylamide (AAm), acrylic acid (AAc) and VCDs. Asymmetric bilayer actuators were then fabricated by the interfacial composition of glycol VCDs polymer gel layer and 3M VHB elastomer layer (Scheme 1b). When immersed in water solutions, the polymer gel will absorb water to induce the formation of hydrophobic VCDs clusters, in which the surficial intramolecular rotations of VCDs are heavily restricted. Consequently, the red aggregation-induced emission of the hydrophobic VCDs clusters is turned on (Scheme 1c). Besides this blue-to-red emission color change, the polymer gel layer also absorbs water to swell, forcing the bilayer actuator to deform into various 3D structures depending on the geometries of the actuators. Importantly, the water-glycol exchange process is also accompanied with a surface tension gradient around the actuator via Marangoni effect, which can be used to promote its autonomous swimming locomotion. On the basis of these

findings, the first octopus-like soft robot was designed by employing eight glycol VCDs gel bilayer actuators as the "octopus arms" and one single glycol VCDs gel as the "octopus head". Its powerful synergistic shape/color change and directional swimming locomotion was also demonstrated.

Results and Discussion

The forefront step in preparing the AIE-active fluorescent gel is the synthesis of CDs coated with rotatable symmetric surfaces, which were prepared from melamine and dithiosalicylic acid according to the previously reported method.[10c] Subsequently, the as-prepared CDs were modified by glycidyl methacrylate (GMA) via a ring-opening reaction to produce the vinyl-functionalized VCDs (Figure 1 a). The TEM image showed a uniform distribution of VCDs with an average diameter of 3–5 nm (Figure 1 b), as is evidenced by the

statistical analysis of their size distribution (Figure S1). Their chemical structures were further verified by Fourier Transform Infrared (FT-IR) and ^{1}H Nuclear Magnetic Resonance (NMR) spectroscopies (Figure S2–5). FT-IR analysis of VCDs revealed a new band at 1720 cm^{-1}, which was attributed to C=O of GMA, while ^{1}H NMR analysis showed that new peaks at 5.5 ppm and 5.7 ppm which were assigned to the chemical signals of the hydrogen of the C=C bond. These results indicated that the polymerizable vinyl groups have been covalently bonded to the surface of VCDs. The VCDs were found to be readily dispersed in common solvents (Figure S6) such as glycol, dimethyl formamide (DMF), dimethylsulfoxide (DMSO) and water, but showing different emission colors in the different solvents. Figure 1 c compares photos of the luminescence of VCDs dispersions in glycol and water. Under 365 nm UV illumination, the transparent glycol solution displayed a blue fluorescence, while the turbid aqueous solution glowed red. The observed results are
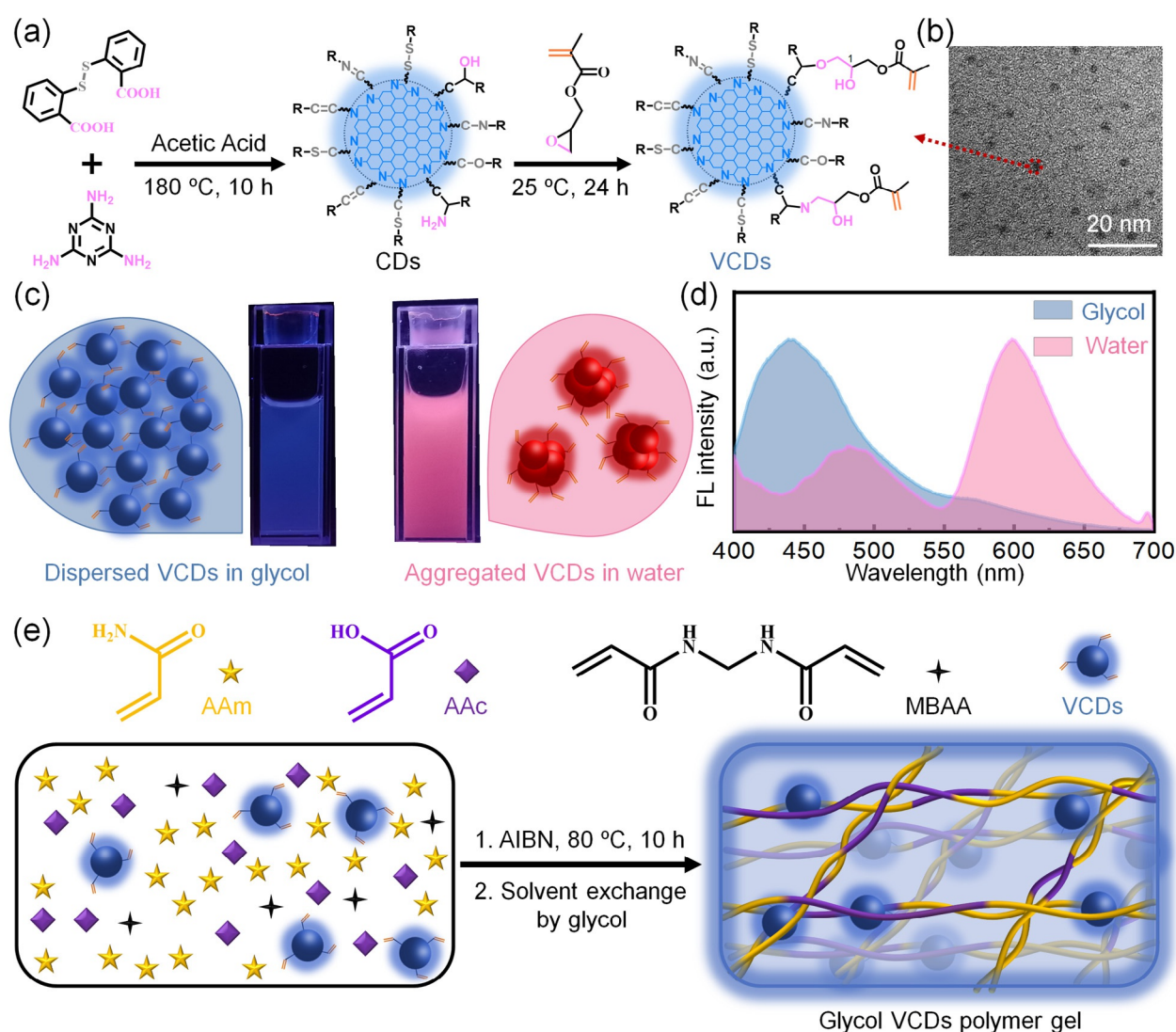

Figure 1. a) Synthetic procedure of CDs and VCDs. b) TEM image of the VCDs. c) Photographs of the VCDs in glycol (0.5 mg mL^{-1}) and in water (0.5 mg mL^{-1}) under 365 nm UV illumination (8 W), as well as the schemes showing the dispersion and aggregation states of VCDs. d) Fluorescence spectra of the VCDs in water (0.5 mg mL^{-1}) and glycol (0.5 mg mL^{-1}) under 365 nm UV illumination. e) Illustration showing the preparation of glycol VCDs polymer gel by the thermo-induced radical polymerization of VCDs, AAm, AAc and MBAA.

consistent with their fluorescence spectra, which showed only a blue emission band centered at 440 nm for the glycol solution, but a new red emission peak around 600 nm for the aqueous solution (Figure 1 d). This observation is believed to be caused by the formation of AIE-active hydrophobic VCDs aggregates in water, as was also evidenced by transmittance (Figure S7) and optical microscope measurements (Figure S8). Consistent with these observations, the VCDs as solids emitted intense red fluorescence and had a strong emission band ranging from 550–700 nm under a 365 nm UV light (Figure S9), further demonstrating the AIE-active nature of VCDs. Additionally, the excited UV light could potentially be promoted to the visible light, because the AIE-active carbon dots (VCDs) used herein have absorption in the visible light range (400–500 nm, Figure S10) and are thus potentially excited by the blue light.

Accordingly, the AIE-active VCDs gel was then prepared by free radical copolymerization of acrylamide (AAm), acrylic acid (AAc), VCDs and N,N′-methylenebisacrylamide (MBAA) with AIBN in DMSO, followed by solvent exchange in glycol (Figure 1 e). The as-prepared glycol gel was blue fluorescent under 365 nm UV light exposure (first photo of Figure 2 a), indicating the homogenous dispersion of VCDs in the cross-linked polymer network. When a round-shaped piece was immersed in water, its fluorescence color gradually changed from blue to rose red due to the solvent-replacement of glycol by water molecules, which proceeds from the edge to the center (Figure 2 c), and vice versa if the solvents are exchanged (Figure S11). This process was also directly observed via in situ Laser Scanning Confocal microscopy (Figure 2 c), which indicated that the VCDs are obviously
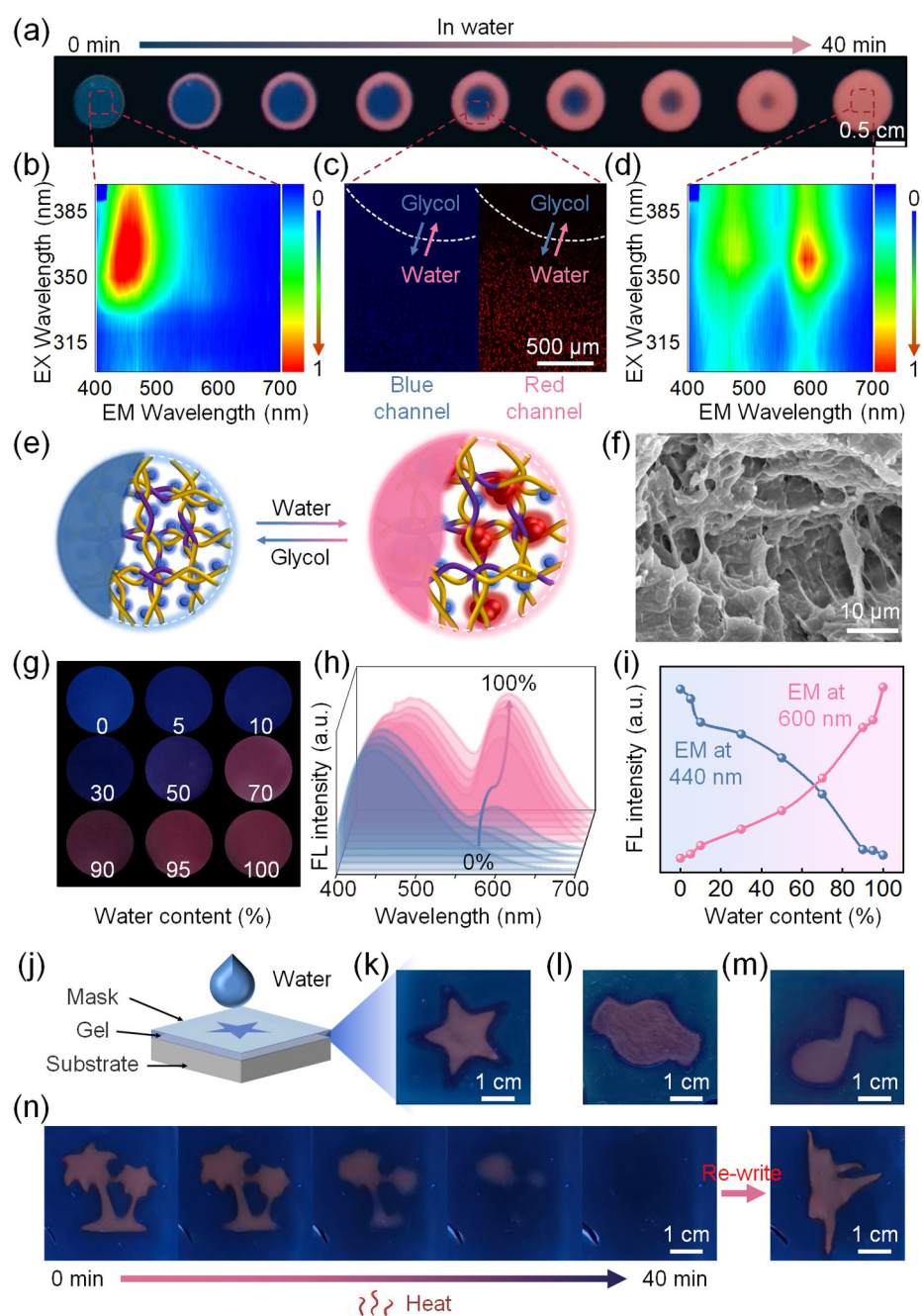

Figure 2. a) Time-dependent photos of the glycol VCDs gel after being immersed in water. b) 3D-fluorescence spectra (λ_{ex} from 300 to 400 nm, λ_{em} from 400 to 700 nm) of the glycol VCDs gel. c) Laser-scanning confocal images of the glycol VCDs gel taken during the water-glycol exchange. The white dotted line is the interface of water-glycol exchange. The blue channel image shows the data gathered from 400–500 nm and the red channel image shows the data gathered from 550–650 nm. Note that the blue spots shown in the blue channel are not the background. They actually come from the blue emission of carbon dots. d) 3D-fluorescence spectra (λ_{ex} from 300 to 400 nm, λ_{em} from 400 to 700 nm) of the water VCDs gel. e) Schemes showing the reversible two-switch-mode fluorescence (blue dispersed fluorescence and red AIE) of the VCDs polymer gel. f) SEM image of the freeze-dried water VCDs polymer gel. g) Photos of the VCDs polymer gel with increasing water fraction from 0% to 100% in the glycol/water gel matrix, as well as their corresponding fluorescence spectra (h) and peak intensity changes at 440 and 600 nm (i). j) Scheme showing the process to print various patterns on the surface of glycol VCDs polymer gel. Photos of the (k) "star", (l) "candy" and (m) "note" patterns on the VCDs polymer gel. n) Photos showing the "writing-erasing-rewriting" process of fluorescent patterns on the gel surface. All photos were taken under 365 nm UV illumination (8 W).

aggregated to result in red fluorescent AIE aggregates along the direction of solvent-replacement. Further, the optical photographs and transmittance spectra also displayed the bright contrast between transparent glycol VCDs gel and opaque water VCDs gel (Figure S12), which implied the phase separation in water of VCDs gels owing to the existence of red AIE aggregates (Figure 2 e). Meanwhile, the SEM analysis of the freeze-dried VCDs gel sample (Figure 2 f) revealed a porous cross-linked network. More evidences for the formation of red-light-emitting aggregates in the polymer network were deduced from the excitation-fluorescence mapping and fluorescence lifetime measurements of glycol and water gel samples. As compared in Figure 2 b and d, a new red fluorescence band was observed at 600 nm after solvent exchange from glycol to water. As shown in Figure S13a, time-resolved photoluminescence lifetime of glycol and water VCDs gels were fitted by mono-exponential and double-exponential decay under the excitation wavelength at 320 nm, respectively. The increased lifetime (from $t_{avg} = 7.943$ ns to $t_{avg} = 40.262$ ns) after the solvent-replacement from glycol to
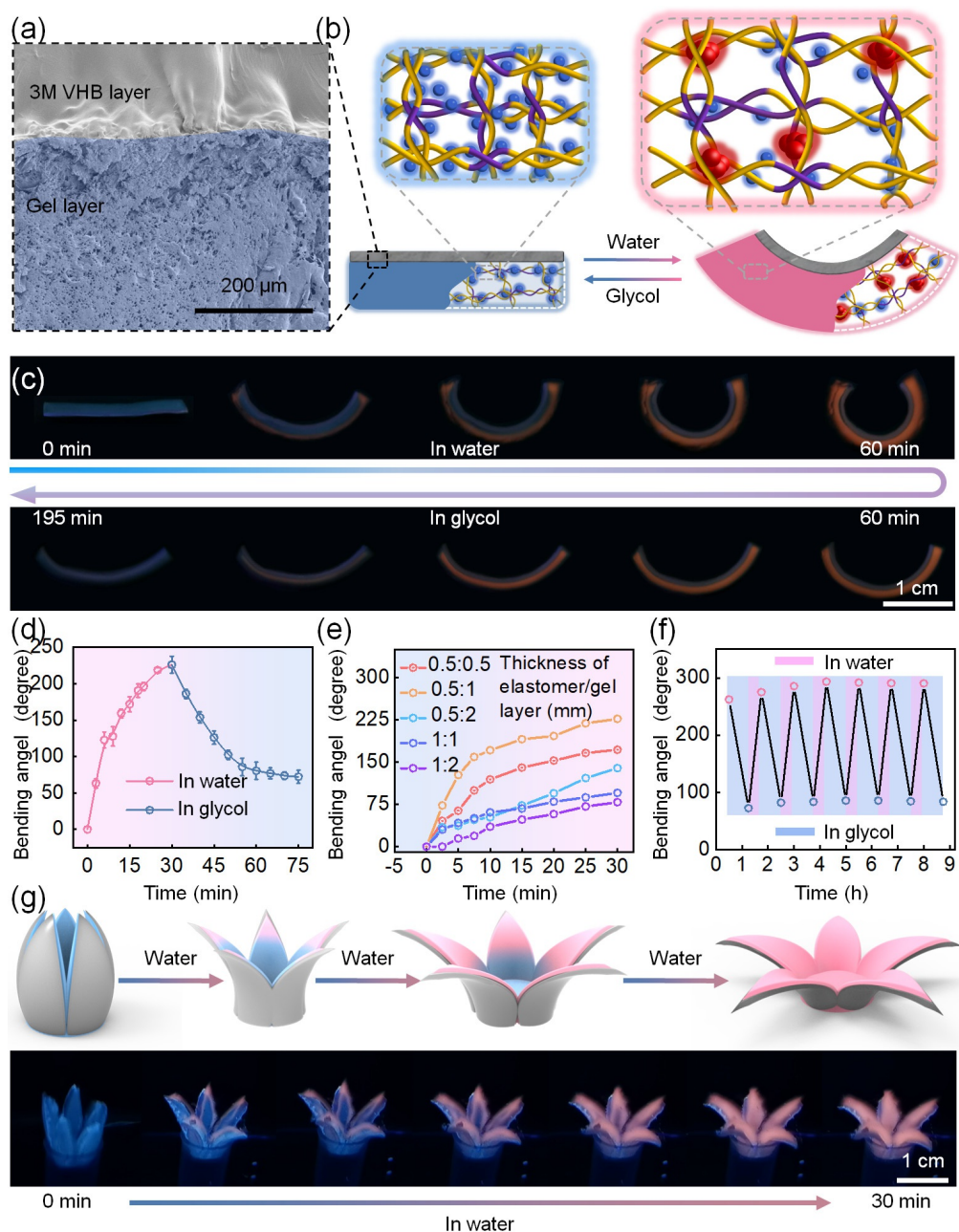

Figure 3. a) Cross-section SEM image of the freeze-dried bilayer VCDs gel actuator. b) Scheme showing the synergistic fluorescence color and shape changes of fluorescent VCDs gel actuator triggered by the water-glycol exchange, as well as the corresponding photos (c). d) Bending angles of the bilayer actuator in water and glycol as a function of time. e) Time-dependent bending angles of the bilayer actuators with different thickness of elastomer and gel layer. f) Cyclic actuating process of the bilayer actuator. g) Schemes representing the simultaneous blooming and blue-to-red color change process of Hydrangea Bush, as well as the corresponding photos of polymer gel-based artificial Hydrangea Bush that display simultaneous blooming and color-changing behaviors. All photos were taken under 365 nm UV illumination (8 W).

water indicated the formation of a new recombination channel (red aggregated state) in the water VCDs gel. In the meantime, the absolute quantum yield of glycol and water VCDs gel were determined to be 1.9% and 3.0%, respectively, when excited at 365 nm, which also demonstrated the formation of red fluorescence-enhanced aggregated states (Figure S13b). In order to further verify its AIE-active nature, the gel samples with different VCDs contents (0.1 wt% to 5 wt%) were prepared, as summarized in Table S1. It was found that red fluorescence intensities of the obtained hydrogels were significantly enhanced with increasing VCDs concentration (Figure S14). More importantly, there was a remarkable red fluorescence enhancement (≈ 8 folds) when increasing the deionized water fraction from 0% to 100% in the glycol/water gel matrix (Figure 2g–i). This result clearly revealed that the formation of more VCDs aggregates in the polymer network was favorable to produce a more intense red fluorescence, as the nature of AIE mechanism would suggest.[6h]

On the basis of this well-established water-triggered blue-to-red fluorescence color-changing behavior, we further explore the potential to print fluorescent patterns on the glycol VCDs gel by using water as the "ink". As illustrated in Figure 2j, various patterns such as a "star" (Figure 2k), a "candy" (Figure 2l) or a "note" (Figure 2m) could be readily printed by adding deionized water onto the pre-designed masks. Remarkably, the printed red fluorescent patterns were found to be stable but completely erased upon heating due to the evaporation of water. As shown in Figure 2n, the "coconut trees" pattern on the VCDs gel faded away upon heating to 60°C for 40 min, allowing for re-printing another information such as a "dancer" pattern on the same gel piece. Moreover, these patterns can also be erased by using glycol to replace the water "ink". These results motivate for a potential application of our VCDs gel system for a "writing-erasing-rewriting" cycle to be used in rewritable paper, information encryption (see Figure S15 for a typical demonstration), or dynamic display.[11]

Afterwards, an anisotropic bilayer actuator was fabricated by employing the fluorescent glycol VCDs gel as the active layer and 3M VHB elastomer as a passive layer (Figure S16) according to the reported fabrication method (see the experimental section for details).[12] Its interfacial composition of the gel layer attaching to the elastomer layer were clearly observed in the SEM image (Figure 3a). Upon exposure to aqueous solutions, the pendent carboxylic groups of the chemically cross-linked poly(AAc-AAm) gel will be partially ionized in the high-dielectric-constant water (Figure S17), resulting in electrostatic repulsion between the polymer chains of the gel. Consequently, the glycol gel layer spontaneously absorbed water to swell, forcing the elastomer layer to deform. As illustrated in Figure 3b and c, the original straight bilayer actuator stripe (20 mm × 3 mm) gradually deformed into an arch shape, that is, bended stripe, within 30 min, accompanied with the obvious fluorescence color change from deep blue to rose red. It is noteworthy that the changes of both shape and color were highly synchronized, because both processes are diffusion-controlled and triggered by the same stimuli (i.e. water-glycol exchange). The syner-

gistic change of shape and color was proved to be reversible after being further immersed again into glycol. In order to quantitatively investigate the shape deformation process of this straight bilayer actuator, time-dependent bending angles were recorded. As summarized in Figure 3d, it was found that the bending angle of fluorescent VCDs gel actuator increased from $\approx 63°$ (3 min) to $\approx 226°$ (30 min) in water and then decreased to $\approx 72°$ again within 75 min in glycol. The reason why the actuating process in water is faster than that in glycol is that the polymer gel has a higher affinity towards the high-dielectric-constant water than the low-dielectric-constant glycol. As a result, the water intake velocity is much faster than the glycol intake velocity. The bending angles of the actuator could be varied by altering the thickness ratio of two bilayers (Figure 3e). The thicker the 3 M VHB layer or the thinner the VCDs gel layer was, the smaller the maximum bending angle became. The reversibility of the solvent-triggered shape deformation of the actuator was confirmed, as shown in Figure 3f. Note that it seems that the bending is not fully reversible in the initial cycles but start to getting more consistent after 2–3 cycles. This observation can be understandable for the following reasons. As detailed in the experimental section (Part 1.3), the chemical crosslinking density of the polymer gel is actually quite low, which means that there remains trace amount of uncrosslinked polymer chains in the gel matrix. In the repetitive actuating experiments (cyclic water-glycol exchange processes), these trace amount of uncrosslinked polymer chains may gradually diffuse out from the gel matrix. After 2–3 actuating cycles, these uncrosslinked polymer chains were completely removed. Consequently, the bending start to getting more consistent after 2–3 cycles.

In nature, many plants are known to display an interesting appearance change in response to some ecological environmental stimuli. One typical example is *Hydrangea Bush*, which are known for their tiny and blue tipped buds in spring that simultaneously bloom and change color from blue to red during the summertime or with a pH change in the soil from acidic to basic. This intriguing natural phenomenon encouraged us to replicate the concerted flower blooming and "blue-to-red" color change by using artificial materials (Figure 3g). To this end, one five-petaled flower was prepared by fixing five glycol gel bilayer actuators into a flower bud. Upon exposure to water stimuli, the blue fluorescent flower bud gradually bloomed along with simultaneous blue-to-red color change, just behaving like the natural *Hydrangea Bush*. This effect was achieved because water molecules gradually diffused into the VCDs gel layer, resulting in both the swelling of gel layer and aggregation of VCDs. As expected, simultaneous red-to-blue color recovery and flower-closing could be triggered upon further exposure to glycol (Figure S18), highlighting the good reversibility of the shape/color changeable behaviors.

Superior to the natural plants, many higher animals such as *Thaumoctopus Mimicus* are not only capable of adjusting their shape and skin color to blend into the surrounding environment, but also have the amazing ability to swim away when there is threat perception. In other words, *Thaumoctopus Mimicus* have evolved to take full advantage of the

synergistic shape deformation, color change and directional swimming motion in order to be disguised from their predators. It was also reported that the directional swimming motion of octopi is controlled by the funnel-shaped organ in the lower part of the head, which can squeeze water out to cause a fast backward swimming.[1f] Inspired by this finding, we further explored the possibility of utilizing the developed glycol VCDs gel to develop swimming robots. As shown in Figure 4a and Movie S1, an equilateral triangle glycol VCDs gel piece (2 mm × 2 mm × 2 mm) moved autonomously for more than 20 min without external energy input after being put on a water surface. This autonomous locomotion process

was accompanied with an obvious blue-to-red color change. The trajectory of this gel swimmer's locomotion in the first 60 s and 1140–1200 s is summarized in Figure 4b and c. We propose that its autonomous locomotion mechanism is based on the solvent-replacement of glycol by water. During the glycol diffusing-out process, a large surface tension gradient (Marangoni Effect) was spontaneously produced around this gel swimmer. It should be noted that the fully hydrated polymer gel cannot swim when put back in glycol. The results are understandable, because glycol has much smaller surface tension, but much larger viscosity than water (Table S2). Therefore, the surface tension gradient (Marangoni Effect),
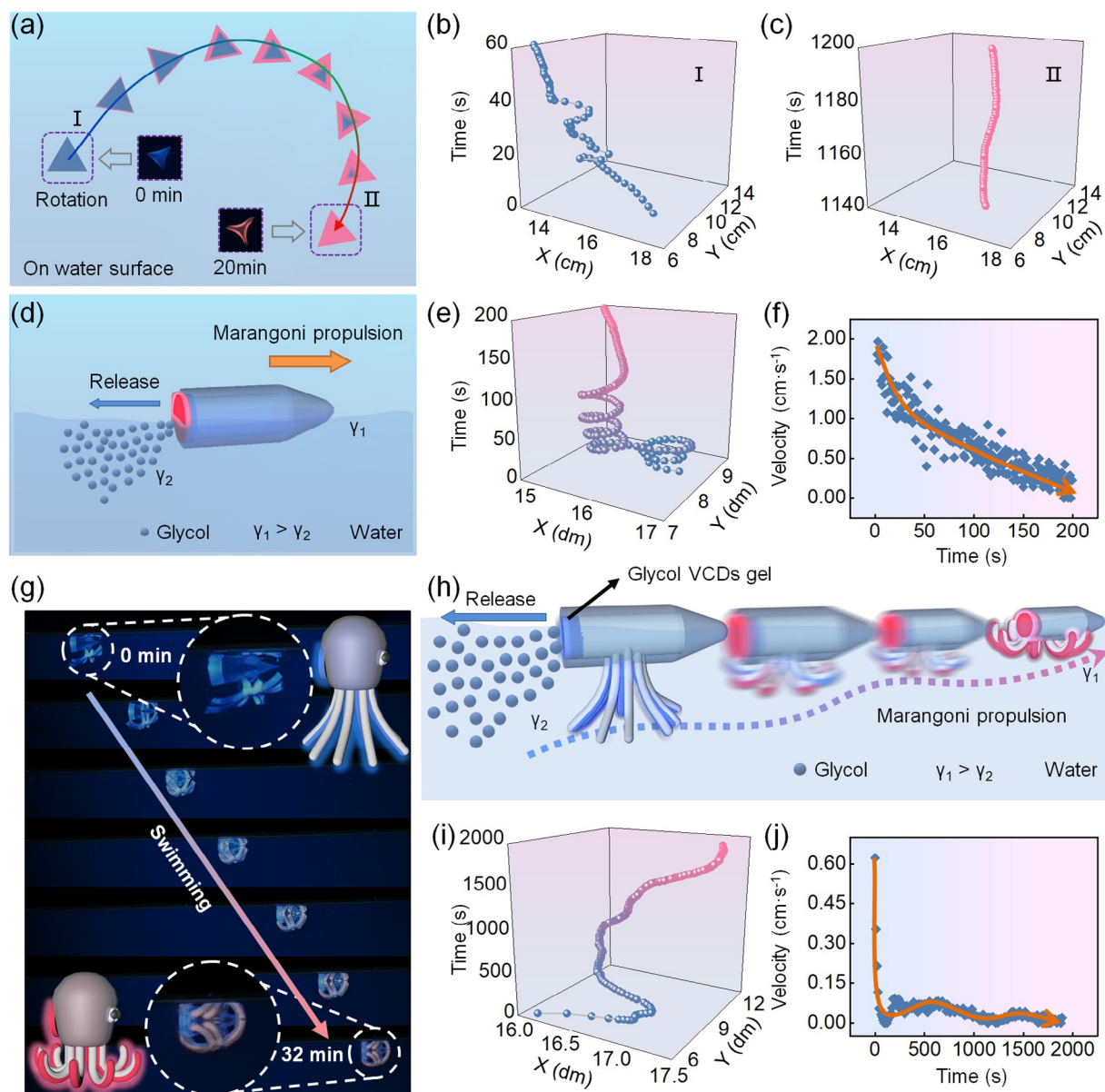

Figure 4. a) Scheme showing the locomotion trajectory of the equilateral triangle VCDs gel. The inset show its photos taken at the beginning and after 20 min under 365 nm UV illumination (8 W). Its motion trajectories of the first 60 s (b) and 1140≈1200 s (c) were depicted quantitatively. d) Scheme showing the locomotion of the "TT-swimmer" on the water surface, which is propelled by the surface tension gradient caused by the release of glycol via Marangoni effect. Its motion trajectory (e) and velocity (f) of the first 200 s were depicted quantitatively. g–h) Photos and schemes showing the synergistic shape/color change and directional swimming locomotion of the VCDs polymer gel-based artificial octopus-like soft robot, as well as its quantitative motion trajectory (i) and velocity (j) of the first 2000 s.

which was caused by water-glycol exchange, was not large enough to enable the locomotion of gel octopus in glycol. However, for this triangle-shaped gel swimmer, its locomotion in water was accompanied with autonomous and fast self-rotation, which lead to a substantial propulsion loss. In order to restrict the self-rotation to result in more efficient locomotion, we were inspired by the idea of the funnel organ design in the head of octopus to produce a new tapered tube swimmer (TT-swimmer) with one fixed glycol VCDs gel at the end (Figure 4d). Owing to this unique design, the self-rotation of gel was completely prohibited. As a result, the designed TT-swimmer was able to move in a circular trajectory with the beginning speed as high as 1.5 cm s^{-1} (Figure 4e,f and Movie S2). With prolonging the time, the released amount of glycol gradually decrease to slow down the locomotion velocity to below 0.5 cm s^{-1} after 100 s. Remarkably, structure of the gel actuator can be further optimized in order to achieve the more accurate directional trajectory, as can be shown in Movie S3. These results suggest that it is theoretically possible to regulate their locomotion trajectories by varying the geometry design of the gel actuators. On the basis of these results, an octopus-inspired swimming gel robot with synergistic shape deformation, color change and directional movement was designed. As schemed in Figure 4h, the gel robot was prepared by employing eight glycol VCDs gel bilayer actuators as the "octopus claws" and one single glycol VCDs gel as the "octopus funnel". The as-prepared gel robot with expanded claws initially looked deep blue, which was similar to the background. On the water surface, the glycol VCDs gel layers of eight claws absorbed water to force these claws to bend, which was accompanied with blue-to-red color change (Figure 4g and Movie S4). Meanwhile, the glycol VCDs gel funnel in the head "squeezed out" glycol to cause a surface tension gradient in the surrounding water environment, which pushed this octopus robot to swim along a tortuous but directional trajectory (Figure 4i, and j). Similarly, the synergistic color/shape changeable process of the gel octopus could be reversed after being further immersed into glycol (Figure S19). In this way, we successfully replicated the tri-function synergistic behaviors of real octopi for the first time by using artificial soft gel materials (although not perfect), paving the route for powerful bio-inspired color/shape changing soft robots.

Conclusion

We have reported the first aggregation-induced emissive CDs polymer gel systems with desirable two-switch-mode fluorescence color (red AIE and blue dispersed fluorescence), which were prepared by covalent incorporation of the hydrophobic CDs coated with rotatable surficial groups into the cross-linked poly(AAm/AAc) network. Anisotropic bilayer actuators were further constructed by interfacially bonding this blue fluorescent glycol VCDs gel layer with a passive 3M VHB elastomer layer (passive layer). Benefiting from the mismatch between the modules and swelling capacities of two layers in water, a *Hydrangea Bush*-inspired bi-functional synergy of flower blooming and blue-to-red color change was

realized by using the developed artificial VCDs gel materials. Furthermore, it was found that a large surface tension gradient was autonomously produced around the bilayer actuator owing to the diffusion of glycol from inside the gel into the surrounding water. These promising advantages further enabled the construction of a powerful octopus-like swimming robot consisting of several straight bilayer actuators as the claws and one homogeneous glycol VCDs gel as the "funnel engine". Its unprecedented ability to accomplish the highly desirable synergistic shape/color change and directional swimming locomotion was verified. Though the octopus-like soft robot demonstrated here are still simple and far from "perfect", with evolution, some more advanced system designs (e.g., one design schemed in Figure S20) could be envisaged for improvement. In conclusion, the developed VCDs gel swimming actuator with tri-function synergy has demonstrated the possibility of bio-inspired intelligent color-changing soft robots, which are expected to be potentially used in environmental applications, aquatic exploration and camouflaging.

Conflict of Interest

The authors declare no conflict of interest.

[1] a) J. S. Sparks, R. C. Schelly, W. L. Smith, M. P. Davis, D. Tchernov, V. A. Pieribone, D. F. Gruber, *PloS One* **2014**, *9*, e83259; b) S. Reiter, P. Hulsdunk, T. Woo, M. A. Lauterbach, J. S. Eberle, L. A. Akay, A. Longo, J. Meier-Credo, F. Kretschmer, J. D. Langer, M. Kaschube, G. Laurent, *Nature* **2018**, *562*, 361–366; c) L. Wang, A. M. Urbas, Q. Li, *Adv. Mater.* **2020**, *32*, 1801335; d) C. A. McLean, A. Lutz, K. J. Rankin, A. Elliott, A. Moussalli, D. Stuart-Fox, *Proc. Biol. Sci.* **2019**, *286*, 20191172; e) Z. C. Ma, X. Y. Hu, Y. L. Zhang, X. Q. Liu, Z. S. Hou, L. G. Niu, L. Zhu, B. Han, Q. D. Chen, H. B. Sun, *Adv. Funct. Mater.* **2019**, *29*, 1903340; f) C. L. Huffard, *J. Exp. Biol.* **2006**, *209*, 3697–3707; g) S. Wei, Z. Li, W. Lu, H. Liu, J. Zhang, T. Chen, B. Z. Tang, *Angew. Chem. Int. Ed.* **2021**, *60*, 8608–8624; *Angew. Chem.* **2021**, *133*, 8690–8706.

[2] a) L. Hu, Y. Wan, Q. Zhang, M. J. Serpe, *Adv. Funct. Mater.* **2020**, *30*, 1903471; b) L. Hu, Q. Zhang, X. Li, M. J. Serpe, *Mater. Horiz.* **2019**, *6*, 1774–1793; c) C. Wang, X. Liu, V. Wulf, M. Vazquez-Gonzalez, M. Fadeev, I. Willner, *ACS Nano* **2019**, *13*, 3424–

3433; d) Y. Sun, L. Chen, Y. Jiang, X. Zhang, X. Yao, S. Soh, *Mater. Horiz.* **2019**, *6*, 160–168; e) Y. Zhou, A. W. Hauser, N. P. Bende, M. G. Kuzyk, R. C. Hayward, *Adv. Funct. Mater.* **2016**, *26*, 5447–5452; f) H. L. Lim, Y. Hwang, M. Kar, S. Varghese, *Biomater. Sci.* **2014**, *2*, 603–618; g) H. Yuk, S. Lin, C. Ma, M. Takaffoli, N. X. Fang, X. Zhao, *Nat. Commun.* **2017**, *8*, 14230; h) S. M. Mirvakili, I. W. Hunter, *Adv. Mater.* **2018**, *30*, 1704407; i) L. W. Xia, R. Xie, X. J. Ju, W. Wang, Q. Chen, L. Y. Chu, *Nat. Commun.* **2013**, *4*, 2226; j) X. Yang, G. Liu, L. Peng, J. Guo, L. Tao, J. Yuan, C. Chang, Y. Wei, L. Zhang, *Adv. Funct. Mater.* **2017**, *27*, 1703174; k) W. Kong, C. Wang, C. Jia, Y. Kuang, G. Pastel, C. Chen, G. Chen, S. He, H. Huang, J. Zhang, S. Wang, L. Hu, *Adv. Mater.* **2018**, *30*, 1801934; l) Z. Lei, Q. Wang, S. Sun, W. Zhu, P. Wu, *Adv. Mater.* **2017**, *29*, 1700321; m) H. Yang, C. Li, M. Yang, Y. Pan, Q. Yin, J. Tang, H. J. Qi, Z. Suo, *Adv. Funct. Mater.* **2019**, *29*, 1901721; n) F. Liu, M. W. Urban, *Prog. Polym. Sci.* **2010**, *35*, 3–23; o) A. F. Greene, M. K. Danielson, A. O. Delawder, K. P. Liles, X. Li, A. Natraj, A. Wellen, J. C. Barnes, *Chem. Mater.* **2017**, *29*, 9498–9508; p) Y. Yang, X. Wang, F. Yang, L. Wang, D. Wu, *Adv. Mater.* **2018**, *30*, 1707071.

[3] a) S. M. Chin, C. V. Synatschke, S. Liu, R. J. Nap, N. A. Sather, Q. Wang, Z. Alvarez, A. N. Edelbrock, T. Fyrner, L. C. Palmer, I. Szleifer, M. Olvera de la Cruz, S. I. Stupp, *Nat. Commun.* **2018**, *9*, 2395; b) A. Choe, J. Yeom, R. Shanker, M. P. Kim, S. Kang, H. Ko, *NPG Asia Mater.* **2018**, *10*, 912–922; c) T. Hessberger, L. B. Braun, R. Zentel, *Adv. Funct. Mater.* **2018**, *28*, 1800629; d) T. Ishiwata, K. Kokado, K. Sada, *Angew. Chem. Int. Ed.* **2017**, *56*, 2608–2612; *Angew. Chem.* **2017**, *129*, 2652–2656; e) Y. Jiang, L. M. Korpas, J. R. Raney, *Nat. Commun.* **2019**, *10*, 128; f) H. Qin, T. Zhang, N. Li, H. P. Cong, S. H. Yu, *Nat. Commun.* **2019**, *10*, 2202; g) A. Mourran, H. Zhang, R. Vinokur, M. Moller, *Adv. Mater.* **2017**, *29*, 1604825; h) J. Meng, G. Wu, X. Wu, H. Cheng, Z. Xu, S. Chen, *Adv. Sci.* **2020**, *7*, 1901931; i) Q. Li, Y. W. Zhang, C. F. Wang, D. A. Weitz, S. Chen, *Adv. Mater.* **2018**, *30*, 1803475; j) S. Wei, W. Lu, X. Le, C. Ma, H. Lin, B. Wu, J. Zhang, P. Theato, T. Chen, *Angew. Chem. Int. Ed.* **2019**, *58*, 16243–16251; *Angew. Chem.* **2019**, *131*, 16389–16397; k) Z. Li, P. Liu, X. Ji, J. Gong, Y. Hu, W. Wu, X. Wang, H. Q. Peng, R. T. K. Kwok, J. W. Y. Lam, J. Lu, B. Z. Tang, *Adv. Mater.* **2020**, *32*, 1906493.

[4] a) Z. L. Wu, M. Moshe, J. Greener, H. Therien-Aubin, Z. Nie, E. Sharon, E. Kumacheva, *Nat. Commun.* **2013**, *4*, 1586; b) H. Chen, F. Yang, Q. Chen, J. Zheng, *Adv. Mater.* **2017**, *29*, 1606900; c) Z. Chen, F. Fu, Y. Yu, H. Wang, Y. Shang, Y. Zhao, *Adv. Mater.* **2019**, *31*, 1805431; d) K. Liu, Y. Zhang, H. Cao, H. Liu, Y. Geng, W. Yuan, J. Zhou, Z. L. Wu, G. Shan, Y. Bao, Q. Zhao, T. Xie, P. Pan, *Adv. Mater.* **2020**, *32*, 2001693; e) H. C. Yu, S. Y. Zheng, L. Fang, Z. Ying, M. Du, J. Wang, K. F. Ren, Z. L. Wu, Q. Zheng, *Adv. Mater.* **2020**, *32*, 2005171; f) Z. Zhao, S. Zhuo, R. Fang, L. Zhang, X. Zhou, Y. Xu, J. Zhang, Z. Dong, L. Jiang, M. Liu, *Adv. Mater.* **2018**, *30*, 1804435; g) Q. L. Zhu, C. F. Dai, D. Wagner, M. Daab, W. Hong, J. Breu, Q. Zheng, Z. L. Wu, *Adv. Mater.* **2020**, *32*, 2005567; h) Q. L. Zhu, C. Du, Y. Dai, M. Daab, M. Matejdes, J. Breu, W. Hong, Q. Zheng, Z. L. Wu, *Nat. Commun.* **2020**, *11*, 5166; i) H. Zhu, B. Xu, Y. Wang, X. Pan, Z. Qu, Y. Mei, *Sci. Robot.* **2021**, *6*, eabe7925.

[5] a) A. Kirillova, R. Maxson, G. Stoychev, C. T. Gomillion, L. Ionov, *Adv. Mater.* **2017**, *29*, 1703443; b) I. Apsite, A. Biswas, Y. Li, L. Ionov, *Adv. Funct. Mater.* **2020**, *30*, 1908028; c) Y. Huang, H. K. Bisoyi, S. Huang, M. Wang, X. M. Chen, Z. Liu, H. Yang, Q. Li, *Angew. Chem. Int. Ed.* **2021**, *60*, 11247–11251; *Angew. Chem.* **2021**, *133*, 11347–11351; d) S. Wang, Y. Gao, A. Wei, P. Xiao, Y. Liang, W. Lu, C. Chen, C. Zhang, G. Yang, H. Yao, T. Chen, *Nat. Commun.* **2020**, *11*, 4359; e) M. Li, X. Wang, B. Dong, M. Sitti, *Nat. Commun.* **2020**, *11*, 3988; f) M. Cheng, F. Shi, *Chem. Eur. J.* **2020**, *26*, 15763–15778; g) M. Xiao, Y. Xian, F. Shi, *Angew. Chem. Int. Ed.* **2015**, *54*, 8952–8956; *Angew. Chem.* **2015**, *127*, 9080–9084.

[6] a) S. Zhu, Q. Meng, L. Wang, J. Zhang, Y. Song, H. Jin, K. Zhang, H. Sun, H. Wang, B. Yang, *Angew. Chem. Int. Ed.* **2013**, *52*, 3953–3957; *Angew. Chem.* **2013**, *125*, 4045–4049; b) S. Tao, S. Zhu, T. Feng, C. Zheng, B. Yang, *Angew. Chem. Int. Ed.* **2020**, *59*, 9826–9840; *Angew. Chem.* **2020**, *132*, 9910–9924; c) Z. Li, L. Wang, Y. Li, Y. Feng, W. Feng, *Mater. Chem. Front.* **2019**, *3*, 2571–2601; d) P. Long, Y. Feng, C. Cao, Y. Li, J. Han, S. Li, C. Peng, Z. Li, W. Feng, *Adv. Funct. Mater.* **2018**, *28*, 1800791; e) B. Zhi, X. Yao, M. Wu, A. Mensch, Y. Cui, J. Deng, J. J. Duchimaza-Heredia, K. J. Trerayapiwat, T. Niehaus, Y. Nishimoto, B. P. Frank, Y. Zhang, R. E. Lewis, E. A. Kappel, R. J. Hamers, H. D. Fairbrother, G. Orr, C. J. Murphy, Q. Cui, C. L. Haynes, *Chem. Sci.* **2021**, *12*, 2441–2455; f) K. Jiang, S. Sun, L. Zhang, Y. Lu, A. Wu, C. Cai, H. Lin, *Angew. Chem. Int. Ed.* **2015**, *54*, 5360–5363; *Angew. Chem.* **2015**, *127*, 5450–5453; g) W. Li, S. Wu, H. Zhang, X. Zhang, J. Zhuang, C. Hu, Y. Liu, B. Lei, L. Ma, X. Wang, *Adv. Funct. Mater.* **2018**, *28*, 1804004; h) J. Mei, N. L. Leung, R. T. Kwok, J. W. Lam, B. Z. Tang, *Chem. Rev.* **2015**, *115*, 11718–11940.

[7] a) C. Y. Li, S. Y. Zheng, C. Du, J. Ling, C. N. Zhu, Y. J. Wang, Z. L. Wu, Q. Zheng, *ACS Appl. Polym. Mater.* **2020**, *2*, 1043–1052; b) Q. Zhu, K. Vliet, N. Holten-Andersen, A. Miserez, *Adv. Funct. Mater.* **2019**, *29*, 1808191; c) B. Sui, X. Zhang, L. Huang, Y. Chen, D. Li, Y. Li, B. Yang, *ACS Sustainable Chem. Eng.* **2020**, *8*, 18492–18499; d) X. Y. Du, C. F. Wang, G. Wu, S. Chen, *Angew. Chem. Int. Ed.* **2021**, *60*, 8585–8595; *Angew. Chem.* **2021**, *133*, 8668–8678; e) Z. Zhu, R. Cheng, L. Ling, Q. Li, S. Chen, *Angew. Chem. Int. Ed.* **2020**, *59*, 3099–3105; *Angew. Chem.* **2020**, *132*, 3123–3129.

[8] a) A. Cayuela, S. R. Kennedy, M. L. Soriano, C. D. Jones, M. Valcarcel, J. W. Steed, *Chem. Sci.* **2015**, *6*, 6139–6146; b) Z. Song, T. Lin, L. Lin, S. Lin, F. Fu, X. Wang, L. Guo, *Angew. Chem. Int. Ed.* **2016**, *55*, 2773–2777; *Angew. Chem.* **2016**, *128*, 2823–2827; c) C. Rizzo, F. Arcudi, L. Dordevic, N. T. Dintcheva, R. Noto, F. D'Anna, M. Prato, *ACS Nano* **2018**, *12*, 1296–1305; d) Q. Lou, S. Qu, P. Jing, W. Ji, D. Li, J. Cao, H. Zhang, L. Liu, J. Zhao, D. Shen, *Adv. Mater.* **2015**, *27*, 1389–1394.

[9] a) X. Chen, Z. Song, S. Li, N. T. Thang, X. Gao, X. Gong, M. Guo, *Green Chem.* **2020**, *22*, 3296–3308; b) S. Bhattacharya, R. S. Phatake, S. Nabha Barnea, N. Zerby, J. J. Zhu, R. Shikler, N. G. Lemcoff, R. Jelinek, *ACS Nano* **2019**, *13*, 1433–1442; c) J. Zhang, J. Jin, J. Wan, S. Jiang, Y. Wu, W. Wang, X. Gong, H. Wang, *Chem. Eng. J.* **2021**, *408*, 127351.

[10] a) J. Luo, Z. Xie, J. W. Lam, L. Cheng, H. Chen, C. Qiu, H. S. Kwok, X. Zhan, Y. Liu, D. Zhu, B. Z. Tang, *Chem. Commun.* **2001**, 1740–1741; b) W. Z. Yuan, Y. Tan, Y. Gong, P. Lu, J. W. Lam, X. Y. Shen, C. Feng, H. H. Sung, Y. Lu, I. D. Williams, J. Z. Sun, Y. Zhang, B. Z. Tang, *Adv. Mater.* **2013**, *25*, 2837–2843; c) H. Yang, Y. Liu, Z. Guo, B. Lei, J. Zhuang, X. Zhang, Z. Liu, C. Hu, *Nat. Commun.* **2019**, *10*, 1789; d) W. Lu, S. Wei, H. Shi, X. Le, G. Yin, T. Chen, *Aggregate* **2021**, *2*, e37.

[11] a) Y. Zhang, X. Le, Y. Jian, W. Lu, J. Zhang, T. Chen, *Adv. Funct. Mater.* **2019**, *29*, 1905514; b) Y. Sun, S. Liu, L. Sun, S. Wu, G. Hu, X. Pang, A. T. Smith, C. Hu, S. Zeng, W. Wang, Y. Liu, M. Zheng, *Nat. Commun.* **2020**, *11*, 5591; c) Y. Liu, Y. Zhang, *ACS Nano* **2021**, *15*, 7628–7637; d) X. Le, H. Shang, H. Yan, J. Zhang, W. Lu, M. Liu, L. Wang, G. Lu, Q. Xue, T. Chen, *Angew. Chem. Int. Ed.* **2021**, *60*, 3640–3646; *Angew. Chem.* **2021**, *133*, 3684–3690; e) Y. Ma, P. She, K. Y. Zhang, H. Yang, Y. Qin, Z. Xu, S. Liu, Q. Zhao, W. Huang, *Nat. Commun.* **2018**, *9*, 3.

[12] Y. Yu, H. Yuk, G. A. Parada, Y. Wu, X. Liu, C. S. Nabzdyk, K. Youcef-Toumi, J. Zang, X. Zhao, *Adv. Mater.* **2019**, *31*, 1807101.